Macromolecules

Article

pubs.acs.org/Macromolecules

Coupled UV−Vis/FT−NIR Spectroscopy for Kinetic Analysis of Multiple Reaction Steps in Polymerizations

Alan Aguirre-Soto,[†] Albert T. Hwang,[†] David Glugla,[‡] James W. Wydra,[†] Robert R. McLeod,[‡] Christopher N. Bowman,[†] and Jeffrey W. Stansbury*[,†,§]

[†]Department of Chemical and Biological Engineering, University of Colorado Boulder, 3415 Colorado Ave., Boulder, Colorado 80303, United States

[‡]Department of Electrical, Computer, and Energy Engineering, University of Colorado Boulder, 425 UCB, Boulder, Colorado 80303, United States

[§]Department of Craniofacial Biology, School of Dental Medicine, University of Colorado, 12800 East 19th Ave., Aurora, Colorado 80045, United States

Supporting Information

ABSTRACT: We couple UV−vis and FT−NIR spectroscopy for the real-time monitoring of polymerization reactions, allowing the simultaneous tracking of the rates of light absorption and initiator/monomer consumption, from which dynamic and previously difficult-to-measure parameters are calculated: quantum yields of initiator consumption, initiation and polymerization, photosensitivity, and residual content of leachable chromophore. Estimating these parameters from one set of experiments is not possible with any other probing technique. We demonstrate the potential of this technique using the free radical initiating system including camphorquinone as photoreducible chromophore and amines as reductants for the visible-light-triggered bulk polymerization of methacrylate monomers, important for dental and biomaterials. Photoinitiation by camphorquinone/amine pairs in two dimethacrylates serves to show the importance of obtaining quantum yields in the polymerizing medium instead of using inert solvents. Additionally, the often-intricate interactions between initiation reactions and the developing macromolecular architectures can be elucidated. For instance, we present the quantification of fluctuations in quantum yields as a function of polymerization. This robust analytical tool with up to millisecond resolution opens opportunities in gaining mechanistic insights from the myriad of macromolecular syntheses available to date.

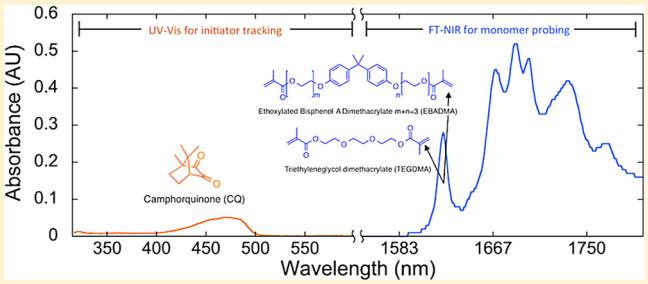

1. INTRODUCTION

Polymerization reactions are receiving considerable attention because polymers provide unparalleled versatility and promise precise control of materials properties.[1] As a result, there has been a rise in the number of routes to macromolecular synthesis, including atom transfer radical polymerization (ATRP),[2] reversible addition−fragmentation chain-transfer (RAFT),[3] copper-catalyzed azide−alkyne cycloadditions (CuAAC),[4] and thiol−Michael reactions.[5] However, understanding of the mechanisms thereof has struggled to keep up because most of these polymer syntheses involve multiple reactions that are interwoven and difficult to characterize with current analytical techniques. Furthermore, the dynamic properties of the medium (e.g., viscosity, refractive index, and light scattering) impose practical restrictions on the analysis of these reactions, which can be dependent on the extent of the polymerization and the particular architecture of the macromolecules formed. Hence, the number of available analytical tools for *in situ* characterization of the rapidly growing polymer chemistry toolbox is relatively limited.[6−9] Herein, we report the coupling of ultraviolet−visible (UV−vis: 250−800 nm) and Fourier transform−near-infrared (FT−NIR: 800−2500 nm) spectroscopy to incorporate analysis of initiators and catalysts to that of the monomer(s) consumption with the goal of providing a better alternative to elucidate the intricate mechanisms of the growing plethora of polymerization reactions.

Most often, the consumption of monomers and/or production of polymer is exclusively evaluated.[10−15] Common discrete techniques are infrared, photoacoustic, Raman, or nuclear magnetic resonance spectroscopy. Continuous analytical methods[16] typically used include calorimetry,[17,18] dilatometry, photothermal,[19] IR radiometry, optical pyrometry,[20,21] and interferometry.[22] Some limitations with these alternatives are that data acquisition is often too slow to analyze the fast reaction rates of many polymerizations[16] and that

Received: July 29, 2015
Revised: September 8, 2015
Published: September 23, 2015

DOI: 10.1021/acs.macromol.5b01685
Macromolecules 2015, 48, 6781−6790

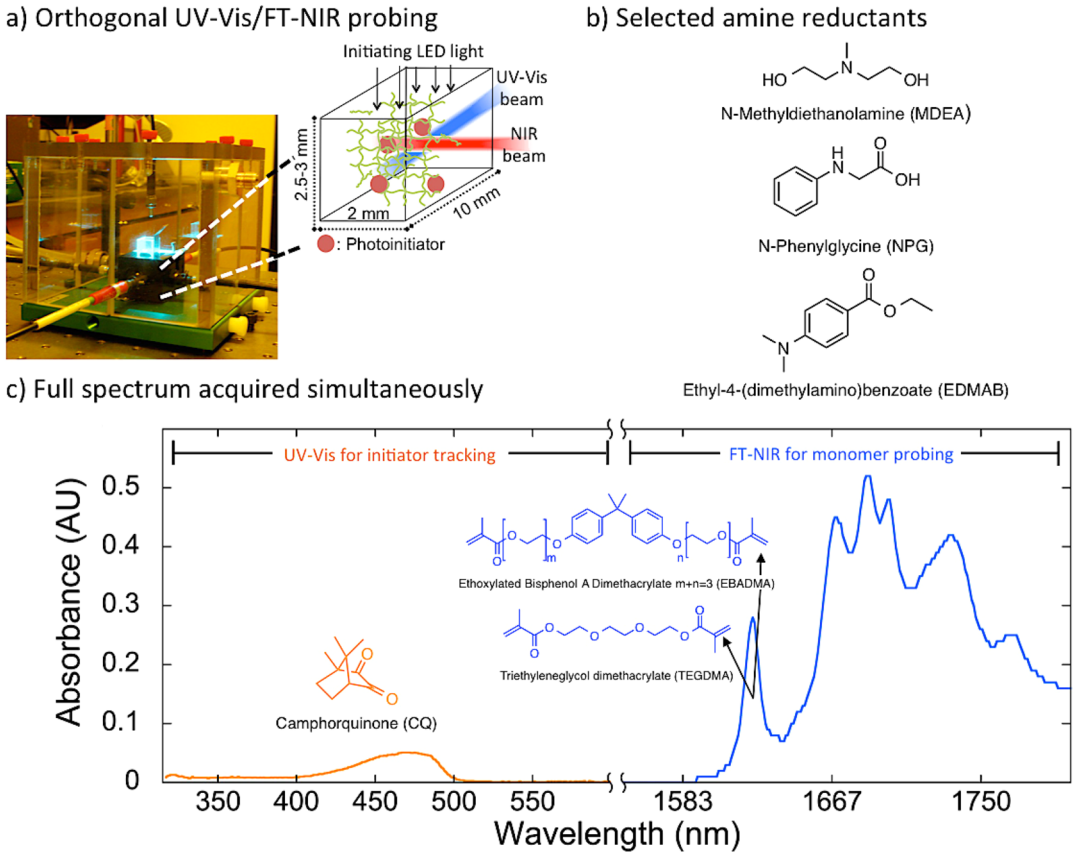

Figure 1. Coupled UV−vis/FT−NIR spectroscopy for analysis of polymerization reactions. (a) Picture of UV−vis/FT−NIR analytical device. (b) Amine reductants chosen for photoreduction of camphorquinone used to initiate chain growth polymerization via the production of alpha-amino alkyl radicals. (c) Full UV−vis/FT−NIR spectrum (300−1900 nm) acquired simultaneously at start of polymerization.

quantification of residual monomer functional groups, now critical in many applications, is precluded. In contrast, real-time FT-IR allows direct determination of conversion as well as indirect estimation of residual functional groups and rate of polymerization (R_p) with up to millisecond resolution without *a priori* knowledge of the enthalpy of the polymerization, as required in calorimetry.[16,23,24] As a result, and due to its ease of use, accessibility, and robustness, FT-IR spectroscopy in several forms is now vital for the assessment of polymerization kinetics.[16,24−29]

FT-IR analysis relies on the quantification of the infrared radiation absorbed by the monomer in either the near-infrared (NIR, 800−2500 nm) or the mid-infrared (mid-IR, 2500−50 000 nm). The use of fundamental absorption bands in the mid-IR region has received more attention than the NIR region.[23] However, mid-IR analyses are restricted in general to thin films or surface analysis mainly because of the high molar absorptivities in this region. It also requires the use of salt plate substrates because glass absorbs strongly in the mid-IR. This precludes the use of glass-based fiber optics for remote probing with mid-IR. In contrast, NIR permits fiber-optic coupled nondestructive probing with convenient sample substrates (e.g., glass or polymers) and more practical sample dimensions.[23,30] Both NIR and mid-IR can be used in transmission, transflection, or reflection mode. But while the first two modes allow quantification of the average bulk monomer content, reflection FT-IR is surface-limited. Similarly, Raman spectroscopy, which is scattering-based, is restricted to a relatively thin layer of the sample due to fluorescence emission. Consequently, FT-NIR in transmission mode is the most versatile technique for fiber optic-coupled, *in situ* probing of bulk monomer concentration allowing integration of initiator (or catalyst) monitoring via other orthogonal techniques.

Real-time *in situ* probing of initiators and catalysts during polymerization remains relatively scarce.[19,31,32] This is mainly due to the fact that these components are not detectable by most analytical instruments at the relatively low concentrations at which they are used. Hence, a lag is still present in mechanistic understanding of the initiation/catalysis pathways and the interplay with monomer and polymer chemistry. Moreover, new initiators and catalysts are constantly being developed for the wide library of monomers.[33−39] This is important because the rational design of initiators and catalysts is becoming a hurdle in the development of polymer syntheses.[40,41] Recently, new insights and theories have been reported on the mechanisms of metal-,[42] organic-,[40] and photocatalysis.[43] However, these require expensive and laborious analytical methods, like isotope labeling,[44] kinetic isotope effects, discrete NMR for light-induced ATRP in solution, or detection of reactive centers with electron paramagnetic resonance spectroscopy (EPR). Hence, a need exists for robust and practical tools to deduce initiation and catalysis mechanisms from kinetic data obtained *in situ* during polymerization reactions.

UV−vis spectroscopy has been seldom employed to analyze initiation or catalysis in polymerizations.[31,32,45−48] The use of UV−vis to monitor these reactions is nontrivial because polymerization causes changes in light scattering and refractive

DOI: 10.1021/acs.macromol.5b01685
Macromolecules 2015, 48, 6781−6790

index that often lead to artifacts in the results, which can preclude acquisition of useful data altogether. Thus, previously reported studies involving analyses of photoinitiator kinetics with UV−vis were limited mainly to reactions in solvent or very dilute monomer solutions, where such problems are mitigated.[48−51] Furthermore, UV−vis radiation has enough energy per photon to trigger undesired photochemical reactions. Hence, a single light beam for both probing and inducing polymerization has been used to avoid premature activation by the probing light. However, this approach restricts the analysis to the usually narrow wavelength range of the frequently unstable light sources that are used to initiate the polymerization.[31,32,46,52] Additionally, UV−vis analysis has been restricted to fixed-wavelength or wavelength-scanning approaches. This type of data acquisition leads to uncertainty in acquisition times, which can be paramount for kinetic analysis.

Herein we present the orthogonal coupling of UV−vis to FT−NIR spectroscopy via fiber-optic-based transmission in the same sample plane perpendicular to the direction of the independent polymerization-inducing irradiation, without prematurely activating the polymerization from exposure to the probing beam, as shown in Figures 1a and 2. Our simultaneous

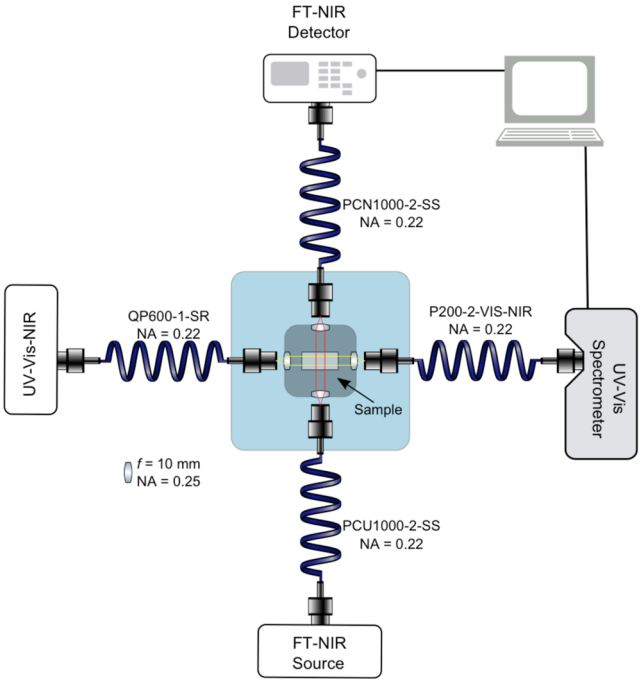

Figure 2. Top view of analytical setup. Orthogonal fiber-optic cables route the UV−vis and infrared probing beams into the detectors through a modified cuvette holder.

full-spectrum UV−vis acquisition (250−1100 nm) allows tracking of multiple absorption peaks (Figure 1c) at precise acquisition time intervals, thus expanding the applicability of real-time UV−vis probing for polymerization reactions. While not required for the reactions studied herein, data can be gathered with up to millisecond resolution in both UV−vis and FT−NIR. This allows direct correlation of initiation and polymerization kinetics for a wide range of practically relevant polymerization reactions. We can successfully obtain useful kinetic data from bulk polymerizations where changes in light scattering and refractive index can be important. This is the first time that UV−vis and FT−IR are coupled directly for polymerization analysis,[24,53,54] and to our knowledge no other methodology has been reported for simultaneous probing of light-induced initiation (or catalysis) and polymerization reaction kinetics.

UV−vis and mid-IR spectroscopies were utilized separately in the only report of both initiation and polymerization kinetics.[53] Separate UV−vis and FT−mid-IR acquisition complicates the direct overlap of the independent results on the same time scale because of the challenge of replicating irradiation conditions and specimen orientations between experiments in different instruments. In contrast, our simultaneous UV−vis/FT−NIR approach eliminates these uncertainties by the concurrent acquisition of initiation/polymerization kinetics data from a single experiment under the same conditions (Figure 1c).

While thermal, redox, or light-induced initiation can be analyzed in our UV−vis/FT-NIR device, we selected a visible-light initiated free radical polymerization. Figure 1b,c contains the structures of the initiator system: camphorquinone (CQ) chromophore and different amines as reductants. We analyzed the polymerizations of two methacrylate monomers and mixtures thereof, used in dental and biomaterials (Figure 1c).[55,56] These formulations are useful to introduce this apparatus while demonstrating its potential to elucidate mechanistic insights. We present results for bulk photopolymerization, but solution-based reactions can also be analyzed. Studies of camphorquinone consumption have been previously reported for CQ/amine pairs in similar monomers and thus serve as a reference to validate the data output from our device.[31,32,46] Most importantly, analysis of these reactions highlights the advantages of the UV−vis/FT−NIR tool for the determination of real-time rates of initiator consumption ($d[CQ]/dt$), polymerization (R_p), and light absorption (I_{abs}); i.e., while the first two rates can be determined with other techniques, I_{abs} can only be directly obtained from UV−vis transmission data. Concurrent evaluation of these three rates permits estimation of the propagation (k_p) and termination (k_t) kinetic constants and the quantum yields of CQ reduction (Φ_{red}), initiation (Φ_i), and monomer polymerization (Φ_p) from the same experiments, as described herein. This allows the assessment of reaction efficiencies for the multiple reaction steps and deduction of complex interwoven mechanisms involved in the polymerization processes. For instance, we show a previously unreported decrease in Φ_{red} as a function of the extent of polymerization of the methacrylate monomers. Not only can these insights aid in the mechanistic understanding of more recently developed light-induced polymer syntheses (e.g., ATRP, RAFT, CuAAC), but it can also expedite the rational improvement of well-established polymerization reactions, as introduced here. This opens new opportunities in light-activated polymer syntheses and holds promise for a variety of other reaction processes as well.

2. EXPERIMENTAL SECTION

2.1. Materials. Ethoxylated bisphenol A-dimethacrylate (EBADMA) with an average degree of ethoxylation of approximately three was provided by Esstech (Essington, PA). Camphorquinone (CQ), ethyl 4-(dimethylamino)benzoate (EDMAB), methyldiethanolamine (MDEA), *N*-phenylglycine (PG), and triethylene glycol dimethacrylate (TEGDMA) were obtained from Sigma-Aldrich (Milwaukee, WI). All reagents were used as received.

2.2. Polymerization-Inducing Irradiation. An eight-wavelength light-emitting diode (LED) unit containing a blue (480 nm; 20 nm fwhm) chip (FC8-LED, Prizmatix, Southfield, MI) was used to induce

DOI: 10.1021/acs.macromol.5b01685
Macromolecules 2015, 48, 6781−6790

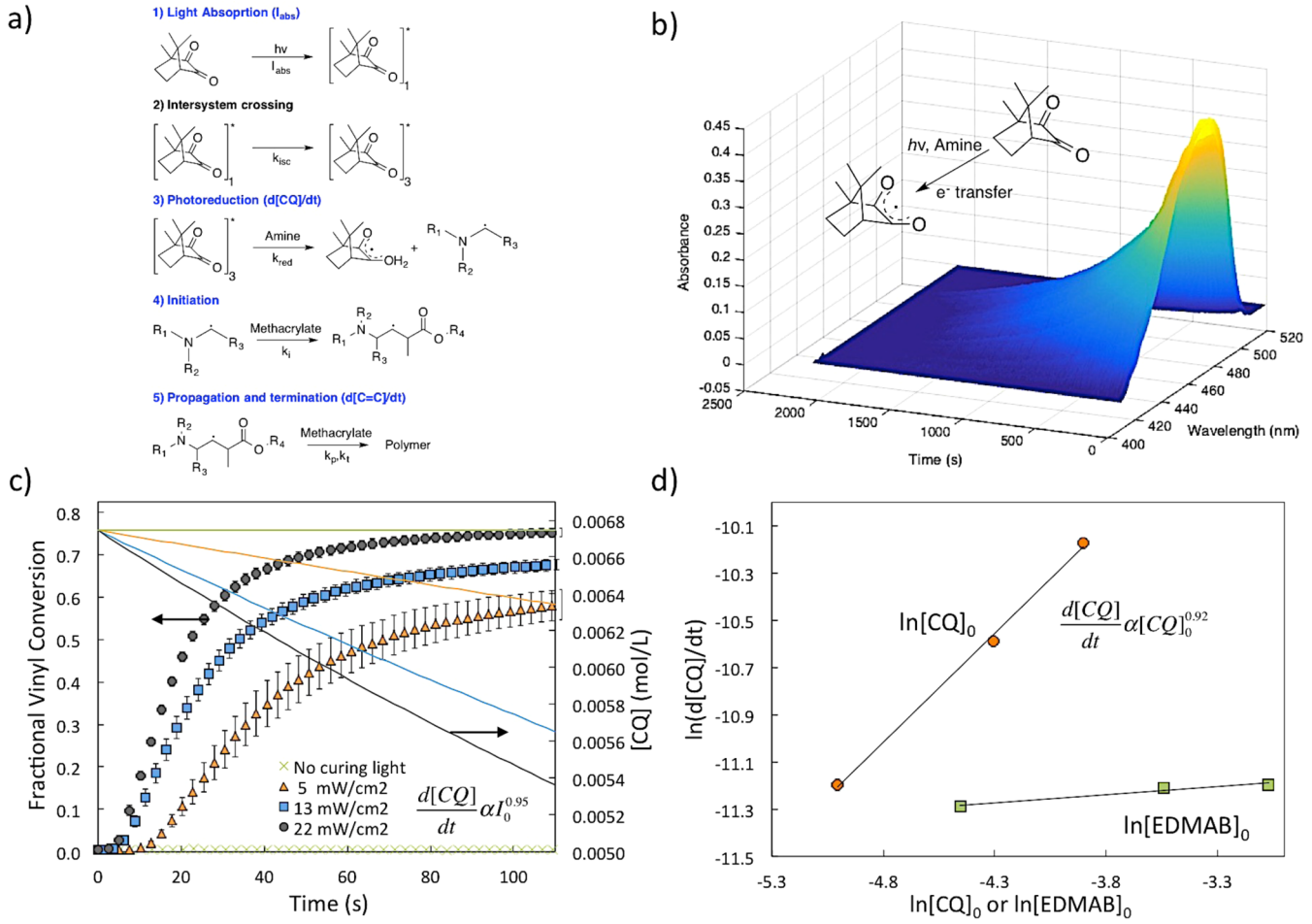

Figure 3. Kinetic analysis of multiple reaction steps during polymerization of EBADMA monomer. (a) Blue-labeled steps are analyzed with the UV−vis/FT−NIR device during chain growth polymerization of methacrylate monomers initiated via photoreduction of CQ by amine. (b) UV−vis absorbance (AU) vs wavelength (nm) vs time (s) showing consumption of $[CQ]_0$= 0.006(7) M during LED irradiation in the presence of $[EDMAB]_0$ = 0.046(4) M. (c) Fractional vinyl conversion and [CQ] vs irradiation time (s), same initial concentrations. (d) d[CQ]/d*t* as a function of $[CQ]_0$ and $[EDMAB]_0$ at 22 mW/cm^2.

the photoreduction of CQ by the amines (Figure 3a). Irradiation intensity was controlled with an internal potentiometer and measured with a radiometer (6253, International Light Technologies, Peabody, MA) designed for the 400−700 nm range. The LED was connected via 1500 μm (internal diameter) fiber-optic cables, collimated (focused) with a SMA-adapted lens from Thorlabs Inc. (Newton, NJ), and placed directly over the PMMA cuvettes (UVette, Eppendorf, Hauppauge, NY). The path length in the direction of the curing irradiation was ∼2.5 mm (Figure 1a), which with the low absorptivity of CQ ensures a valid thin-film approximation for all experiments.

2.3. Coupling UV−Vis to FT−NIR. The UV−vis and FT−NIR beams were coupled into a SMA-fitted cuvette holder (CUV-ALL-UV 4-Way Cuvette Holder, Ocean Optics, Dunedin, FL) that holds the dual-path length PMMA cuvette. Rain-X was used to pretreat the cuvettes to prevent signal losses from heterogeneous delamination of the bulk poly methacrylates from the cuvette. A sample volume of ∼50 μL was used with dimensions of 2 mm × 10 mm × 2.5 mm, although other cuvette configurations can be accommodated as needed. The longer path length was used for UV−vis to prevent saturation of the NIR signal from bulk monomer samples. UV−vis/FT−NIR beams were transmitted orthogonally within a matched horizontal plane through the center of the sample at an approximate depth of 1.25 mm using multimode fiber-optic cables. The aperture of the UV−vis probing beam was reduced with a pair of ∼ 0.5 mm pinholes positioned at a ∼1.25 mm height (center) to reduce the amount of light from the polymerization-inducing LED that reaches the UV−vis detector and to prevent premature activation of the reaction by the low-intensity UV−vis probing beam (Figure 2). Prepared samples were isothermally sonicated for 10 min prior to every experiment.

Monomer conversion was monitored with an FT−IR spectrophotometer (Nicolet Magna-IR Series II, Thermo Scientific, West Palm Beach, FL) by following the peak area of the first overtone absorption band of the =CH$_2$ bonds (∼6167 cm^{-1} = 1621 nm). Monomer absorbance was confirmed to fall within the linear Beer−Lambert region for the concentrations and path length utilized. The spectrophotometer is equipped with an extended range KBr beam splitter and an InGaAs detector. The NIR signal was transmitted to/from the remote specimen via matched 1000 μm (i.d.) fiber-optic cables. The FT−IR settings were set to 8−16 scans, a resolution of 8, an optical gain of 1, and an optical aperture of 3−5. The velocity of the interferometer was adjusted according to the desired acquisition time.

Fiber-optic coupled fixed-grating spectrometers: UV−vis detectors USB2000-UV-vis and USB4000-FL (miniature fiber-optic spectrometers, Ocean Optics, Dunedin, FL), equipped with a Czerny−Turner configuration and a charge-coupled device (CCD) were employed. These advancements allow 10−100 Hz resolved full spectra acquisition (accounting for scan averaging) because no moving parts are involved. However, other modifications to similar spectrometers have reported to achieved 1 kHz resolution. A 1500 μm (i.d.) incoming fiber cable and a 50 μm (i.d.) receiving cable were used for the UV−vis. The change in the absorbance between 400 and 510 nm is related to the n → π^* transition of the carbonyl groups in CQ, which decays as a function of CQ concentration. The CQ absorbance was calibrated against concentration to confirm that it also follows Beer−Lambert's

DOI: 10.1021/acs.macromol.5b01685
Macromolecules 2015, 48, 6781−6790

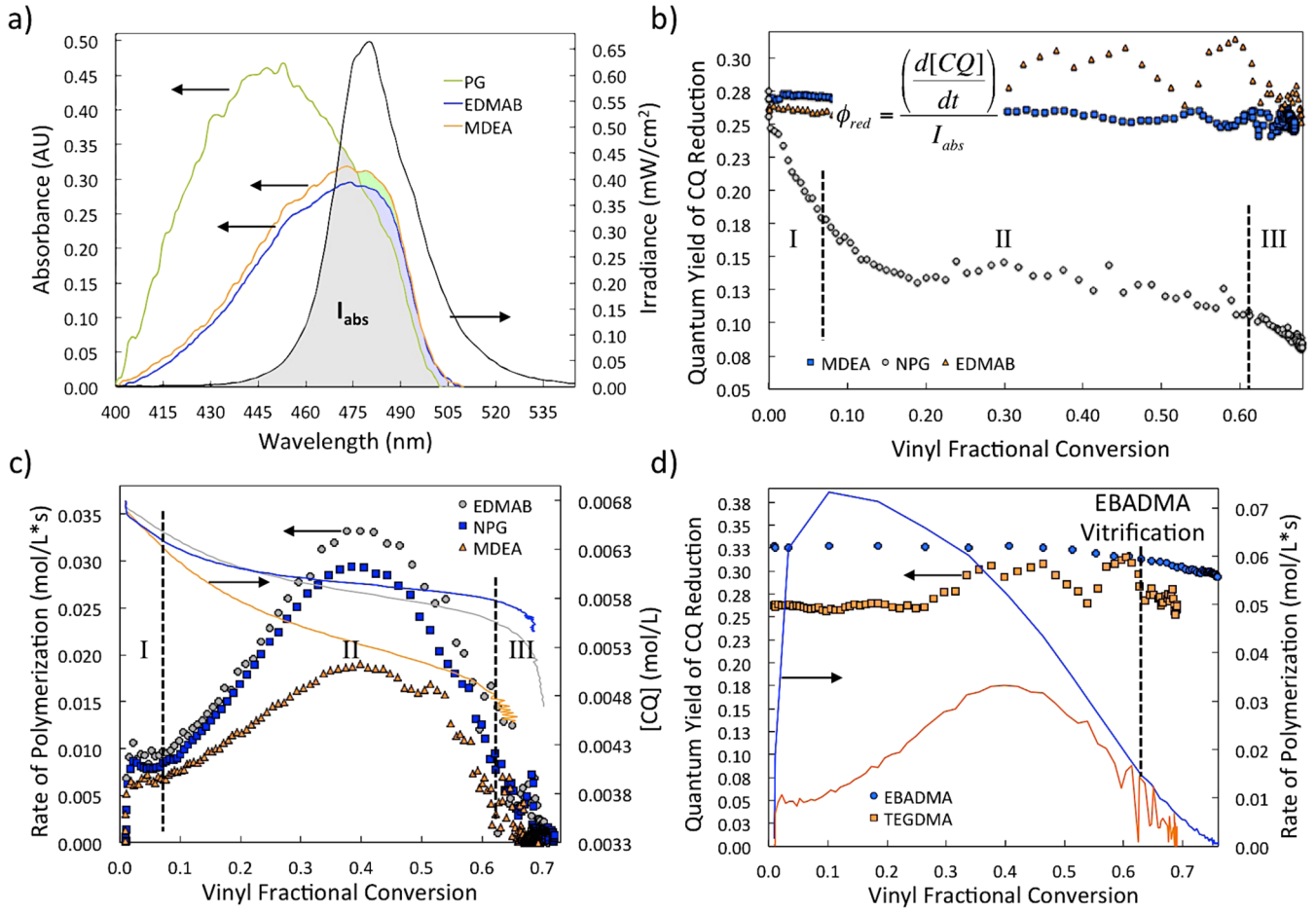

Figure 4. Simultaneous determination of the rates of polymerization and photon absorption and polymerization, CQ consumption, and CQ photoreduction quantum yields. (a) Initial UV−vis absorbance spectra in TEGDMA; $[CQ]_0$ = 0.00674 M and $[amine]_0$ = 0.0464 M. Secondary *y*-axis corresponds to LED emission. (b) Quantum yield of CQ reduction (Φ_{red}) as a function of vinyl fractional conversion. (c) Rate of polymerization (R_p) of TEGDMA and [CQ] as a function of conversion. (d) Quantum yield of CQ reduction (Φ_{red}) and R_p vs conversion; $[CQ]_0$ = 0.00674 M and $[EDMAB]_0$ = 0.0464 M at 22 mW/cm^2.

linearity. The high sensitivity USB4000-FL permits the use of very low intensity UV−vis light in continuous or pulsed mode to probe samples without prematurely initiating the polymerization (Figure 3c). Integration time was set to 50−100 ms with 10 scans to average and a boxcar width of 3. The intensity of the UV−vis probing beam was set to the same initial photon count for every experiment in the SpectraSuite software. Negligible polymerization occurred from extended exposure to the UV−vis probing beam from stable halogen sources emitting on the order of 10^1−10^2 μW/cm^2 (Figure 3c), e.g., DH-Mini light source (Ocean Optics, Dunedin, FL) with an emission spectrum restricted to 400−700 nm.

2.4. Spectral Analysis. The FT-NIR results were obtained directly from the OMNIC Software (Thermo Scientific, West Palm Beach, FL) and processed in Excel according to the method reported by Decker; peak area was between 6259.9 and 6101.8 cm^{-1}.[16] The UV−vis output was collected with the SpectraSuite Software (Ocean Optics, Dunedin, FL). A FORTRAN code was written to merge the data into a single text file. Then a MATLAB script was written to process the full-spectrum absorbance, remove any baseline shifts associated with optical attenuation by light scattering and refraction of the UV−vis probing beam (Figure S1), and extract the absorbance maximum λ_{max} (~470 nm); i.e., maximum absorbance was found for every spectrum and plotted against time. The maximum absorbance point in the data fluctuated randomly and negligibly (±2 nm). At least three replicates were performed for each experiment. Averaged data were then fitted to exponential equations using MATLAB curve fitting tool. R^2 values for all fittings were at least 0.94.

3. RESULTS AND DISCUSSION

3.1. Validity of UV−Vis/FT−NIR Data Output. Figure 3a shows key reaction steps of the light-induced chain growth polymerizations selected for this introductory work: (1) absorption of light between 400 and 500 nm to convert ground-state CQ into an excited-state singlet, (2) intersystem crossing from an excited singlet into a triplet state CQ, (3) reduction of the excited triplet CQ by the ground-state amine, (4) initiation of the methacrylate monomer by the α-aminoalkyl radical formed, and (5) lumped propagation/termination steps involving the monomer-based radicals. The blue-labeled steps are those for which information can be deduced with our UV−vis/FT−NIR device. The photophysical transitions, e.g. fluorescence and intersystem crossing (Figure 3a, step 2), require more expensive transient laser, pump−probe spectroscopy, or flash photolysis, which are typically performed in inert solvents and under a narrow set of conditions because these photophysical steps involve significantly shorter-lived intermediates and their detection can be affected by the polymerizing medium. Nevertheless, simultaneous analysis of the blue-labeled reaction steps is presented here for the first time and provides more information per experiment than other instrumental approaches.

DOI: 10.1021/acs.macromol.5b01685
Macromolecules 2015, 48, 6781−6790

The CQ absorbance spectrum (λ_{max} at around 470 nm) correlates linearly with CQ concentration within the values of $[CQ]_0$ used here. The slope of this correlation is the molar extinction coefficient and was determined to be ~35 ± 1 (M^{-1} cm^{-1}) in bulk TEGDMA and EBADMA monomers, which agrees well with prior characterization of CQ in solvents.[45,52] Figure 3b shows a 3D plot of the light absorbance between 400 and 520 nm as a function of time (s) and wavelength (nm). The spectra shown have been processed to eliminate the shift in the baseline that was observed for all samples. The latter is due to changes in light scattering and refraction associated with density fluctuations and changes in properties during polymerization. These factors affect the amount of light transmitted through the samples into the UV−vis detector, thus causing fluctuations in the baseline of the absorbance spectra. We include the uncorrected 3D spectra plot in Figure S1. A similar baseline correction is routinely performed in the real-time FT-IR analysis of polymerization reactions by the software provided with the IR spectrophotometers, as used herein. Despite these baseline shifts, all UV−vis and FT−NIR absorbance raw data remained under the saturation limits of the detectors during the reaction.

CQ photoreduction rates were fitted to the expected single-exponential kinetic expressions ($R^2 \geq 0.94$) derived from the proposed mechanism (Figure S2).[57−59] The half-lives of CQ were in reasonable agreement with those reported by others.[31,32] Then, scaling factors were determined for the effects of irradiance and initial concentrations. Figure 3c confirms that the rate of CQ photoreduction by EDMAB reductant scales linearly with incident irradiation intensity ($d[CQ]/dt \propto I_0^{0.95}$; $R_2 = 0.98$),[58] whereas the initial rate of polymerization (R_{p0}) for EBADMA was found to have the expected 1/2 order dependence on I_0 ($R_p \propto I_0^{0.54}$; $R_2 = 0.96$). Additionally, Figure 3c shows that no CQ consumption or polymerization was observed in the absence of the polymerization-inducing LED irradiation; i.e., the UV−vis probing beam does not promote the initiation reaction in this time scale.

Then, we confirmed the first-order dependence of $d[CQ]/dt$ on $[CQ]_0$ at 22 mW/cm^2 in EBADMA (Figure 3d), while R_p increased until a certain threshold value with increasing $[CQ]_0$, as reported by Cook and Pyszka and co-workers.[56,60,61] Within the concentrations used for this study $d[CQ]/dt$ was observed to be independent of $[EDMAB]_0$, as observed when the amine reductant is used in excess. R_{p0} for EBADMA also remained roughly constant with increase in $[EDMAB]_0$.

3.2. Calculation of Quantum Yields. The quantum yields of initiator consumption (Φ_d), primary radical (e.g., α aminoalkyl) production (Φ_r), monomer initiation (Φ_i), and polymerization (Φ_p) are defined as the ratio of the rates of either initiator consumption (Figure 3a, step 3), primary radical production (Figure 3a, step 3), production of monomer-based radicals (Figure 3a, step 4), or polymerization of functional groups (Figure 3a, step 5) over the rate of photon absorption I_{abs} (Figure 3a, step 1). Hence, knowledge of I_{abs} is absolutely required and can only be obtained with UV−vis spectroscopy. To quantify I_{abs}, i.e., the overlap between the absorbance spectrum of the initiator (CQ) and of the emission spectrum of the polymerization-inducing light (LED), is detailed in the Experimental Section and shown in Figure 4a. We recently used this method for the calculation of quantum yields of photolysis of photobase generators.[62] When using polychromatic light sources, I_{abs} is most often not accounted for because it requires full-spectrum integration in the UV−vis region where absorbance and emission overlap. Thus, I_{abs} determination has been mostly limited to cases in which monochromatic laser irradiation is used to trigger the polymerization reaction because one-wavelength activation solely requires knowledge of the initial concentration of the light-absorbing initiator and the molar absorptivity at single emission wavelength (ε) as well as the path length of the sample. Then, the absorption is frequently assumed to be constant throughout the polymerization on the grounds that the initiator concentration varies only slightly during the polymerization.[63,64] In contrast, we can determine I_{abs} for any broad-spectrum irradiation light source and without assuming a constant initiator concentration throughout the experiments.

Furthermore, our UV−vis/FT−NIR apparatus provides the advantage of determining I_{abs} in the actual monomer/polymer as opposed to previous analyses of the photochemical reactions in inert solvents.[45,65] It is well-known that absorbance spectra, and thus I_{abs}, depend on the electronic and resonance characteristics of the solvent (confirmed in Figure S3). Hence, obtaining I_{abs} in the actual polymerizing medium provides an unparalleled advantage over other analytical methods.

Initial I_{abs} for solutions of EDMAB, MDEA, or NPG in monomer were 3.53×10^{-8}, 4.17×10^{-8}, and 4.51×10^{-8} einstein/(cm^3 s), respectively. These values equate to 10, 12, and 13% absorption of the incident irradiation ($I_0 = 3.53 \times 10^{-7}$ einstein/(cm^3 s)), which allows us to assume that the concentration of photons is effectively uniform with depth. Light emission from the LED has a Gaussian distribution, but the samples were centered relative to the light beam to ensure a homogeneously exposed sample cross section.

Here, for example, we show that the amine reductant can affect the CQ absorbance spectrum (Figure 4a). We observed that methyldiethanolamine (MDEA) provides a slight enhancement in the CQ molar absorptivity value as compared to analogous solutions of the other amines in monomer. On the other hand, the absorbance spectrum of CQ with NPG not only increases significantly, but is also blue-shifted by roughly 20 nm. The latter result indicates the formation of a ground-state complex since even though NPG also absorbs light in the 400−500 nm region, the spectrum of CQ/NPG solutions is not represented by the addition of the CQ and NPG individual spectra (Figure S4). These media-based differences in I_{abs} are frequently ignored in the analysis of light-induced polymerization reactions but can be readily addressed with our UV−vis/FT−NIR technique.

Accounting for these differences in I_{abs}, we calculated the quantum yield of CQ photoreduction (Φ_{red}) as $d[CQ]/dt$ over I_{abs} as a function of time/monomer conversion (Figure 4b) in TEGDMA. Initial Φ_{red} values for EDMAB, MDEA, and NPG (0.26 ± 0.02, 0.27 ± 0.02, and 0.29 ± 0.01, respectively) are in reasonable agreement with the quantum yields reported in inert solvents (e.g., ethyl acetate).[65] These values correlate linearly with the oxidation potentials of the amine reductants: 1.1 (EDMAB), 0.9 (MDEA), and 0.4 eV (NPG), as expected. However, more experiments are needed to verify if Φ_{red} correlates primarily to the oxidation potentials of the amines or if there is also a significant contribution of the proton (H^+) donation capability, pK_a, of the semireduced intermediates. A systematic study of a broader range of amine reductants can address this question, but here we want to introduce the UV−

DOI: 10.1021/acs.macromol.5b01685
Macromolecules 2015, 48, 6781−6790

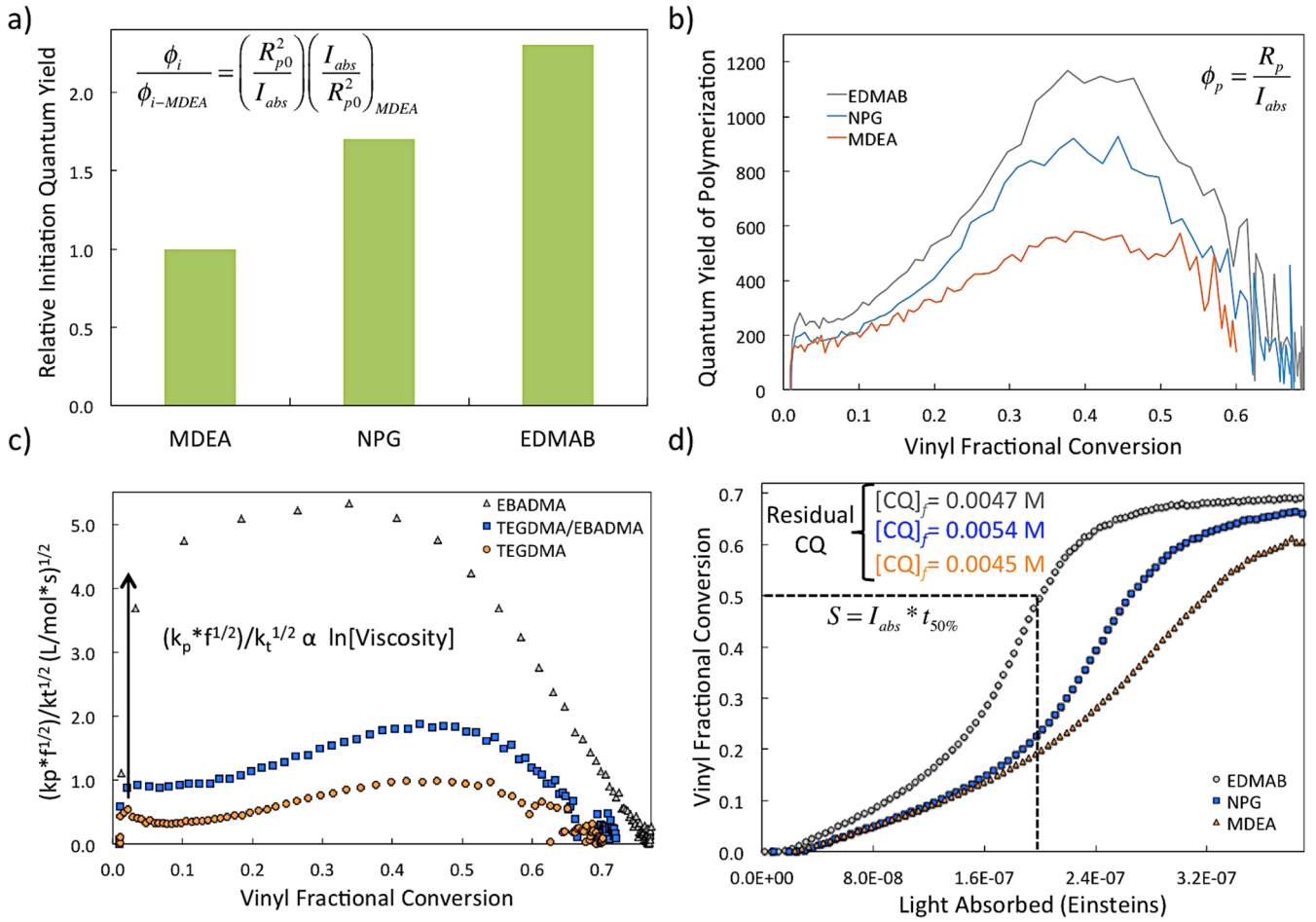

Figure 5. Quantum yield of polymerization, polymerization kinetic constants, CQ photoreduction, and photosensitivity from a single experiment set. (a) Relative quantum yields of monomer initiation ($\Phi_i/\Phi_{i\text{-}ref}$) by the α-aminoalkyl radicals formed (Figure 3a, step 4). (b) Quantum yield of polymerization (Φ_p) of TEGDMA monomer as a function of vinyl fractional conversion; $[amine]_0$ = 0.0464 M, $[CQ]_0$ = 0.00674 M at 22 mW/cm^2. (c) Ratio of the propagation (k_p) and termination ($k_t^{1/2}$) kinetic constants times initiation efficiency factor, f, as a function of conversion. (d) Vinyl fractional conversion vs total photons absorbed (einsteins = mol of photons/L) in TEGDMA. Residual camphorquinone $[CQ]_f$ as estimation of leachable potentially cytotoxic molecules.

vis/FT−NIR capabilities and potential to investigate such differences in efficiencies of photochemical reactions.

Despite the reasonable agreement in the initial Φ_{red}, the results in Figure 4b show Φ_{red} can fluctuate throughout the polymerization, counter to what was previously thought.[45] EDMAB reductant gave a negligible decrease in Φ_{red} as a function of conversion. However, MDEA shows a noticeable decrease in the photoreduction quantum yield, which appears to decrease linearly with vinyl fractional conversion. However, NPG was the most interesting case. While the initial Φ_{red} with NPG was the highest at the very beginning of the reaction, it drops dramatically from 0.29 to 0.20 by the time the gel effect or autoacceleration region (~4−5% conversion) is reached in the homopolymerization of TEGDMA. Then, as the bulk polymer approaches vitrification at around 62% vinyl conversion, based on the inflection point in the R_p curve[66] (Figure 4b,c), Φ_{red} decays more steeply to a value of only 0.08−0.06. Ultimately Φ_{red} decreased by almost 4 times by the time the limiting vinyl conversion is reached. We labeled these transitions (I, II, and II) separated by black dashed lines in Figures 4b and 4c and propose that these are more drastic in the case of the NPG reductant because of its higher polarity relative to MDEA and EDMAB. TEGDMA monomer has a relatively low polarity, which decreases further with polymerization. Hence, the solubility, and thus, homogeneity, will be poorer for NPG during the polymerization. In fact, we observed that a longer isothermal sonication was required to get equimolar amounts of NPG into the TEGDMA solutions before polymerization.

These results show that in general Φ_{red} can be affected by mobility as the polymerization progresses. Figure 4d shows that while Φ_{red} remains fairly constant during the polymerization of TEGDMA (monomeric T_g = −85 °C)[67] with CQ/EDMAB, it actually decreases slightly toward the end of the polymerization of the higher T_g (i.e., less mobile) EBADMA (T_g = −42 °C).[67] Moreover, Cook reported that d[CQ]/dt with *N*,*N*-3,5-tetramethylaniline remains constant despite changes in initial viscosity and final mechanical properties.[58] Our results indicate that the initiation by the bimolecular photoreduction reaction could be affected by the mobility of the developing macromolecular structure in some formulations, but additional experiments in controlled solvents and monomers are required to determine the validity and extent of this hypothesis.

Additionally, if the photoreduction of CQ can be assumed to be the only reaction leading to the disappearance of the CQ UV−vis peak (step 3 in Figure 3a), and we know the amount of

DOI: 10.1021/acs.macromol.5b01685
Macromolecules 2015, 48, 6781−6790

primary radicals produced per photoreduced CQ (n), then the quantum yield of primary radical production Φ_r can be estimated as $\Phi_{red}{\cdot}n$; i.e., for the reactions studied here we know that we can assume that every CQ that is photoreduced leads to two primary radicals (a ketyl and an α-aminoalkyl). Hence, in this case we could multiply $\Phi_{red}{\cdot}2$ to obtain the quantum yields of primary radical production with values of 0.52, 0.54, and 0.58 for EDMAB, MDEA, and NPG, respectively. However, with these CQ-based exemplar formulations Φ_r has to be divided by two assuming the ketyl radical does not initiate polymerization. In cases like phosphine oxides and acetophenones though multiple initiating primary radicals are produced per initiator cleaved, which can be captured by this method.

Direct determination of the quantum yield of monomer initiation (Φ_i) remains scarce because quantification of the short-lived monomer-based radical concentration requires sophisticated instrumentation (e.g., pulsed laser polymerization−size exclusion chromatography, PLP−SEC) performed under a very narrow set of conditions and limited to low monomer conversions.[68−70] Hence, relative $\Phi_i/\Phi_{i\text{-ref}}$ ratios have been proposed to circumvent these issues. However, even determination of $\Phi_i/\Phi_{i\text{-ref}}$ is limited because it requires knowledge of R_p and I_{abs}, which can only be obtained simultaneously with an approach such as the UV−vis/FT−NIR tool described here; i.e., Raman spectroscopy tracks peaks for multiple molecules, but photons from the initiating irradiation preclude continuous measurement of the weak Raman signals. We show that we can readily determine $\Phi_i/\Phi_{i\text{-ref}}$ values with our UV−vis/FT−NIR analytical apparatus (Figure 5a) to assess the relative efficiency of the primary radicals produced (Figure 3a, step 3) in initiating the polymerization of the monomer by radical attack (Figure 3a, step 4). We found that the relative trend is EDMAB > NPG > MDEA, which agrees with previous reports of relative reactivity that were based exclusively on R_p analysis. It is important to acknowledge that NPG has been reported to initiate polymerization more efficiently in other monomer/solvent combinations, which can be related to the fact that NPG is more compatible with higher polarity monomers or water-based polymerizations. Also, it is worth noting that $\Phi_i/\Phi_{i\text{-ref}}$ is calculated from initial R_p (R_{p0}) and I_{abs} because the equation for $\Phi_i/\Phi_{i\text{-ref}}$ depends on the assumption of equivalent propagation and termination kinetic constants.

Additionally, the quantum yield of polymerization (Φ_p) can be obtained as R_p/I_{abs} (Figure 5b). Φ_p values with the three amine reductants in TEGDMA at 22 mW/cm^2 were found to be in the low-end of the typical range for photopolymerizations performed under air (200−13 000), i.e., without inert gas purging.[71] Using these values to assess the reactivity of the amines tested, they rank EDMAB > NPG > MDEA, where EDMAB reached 1200, NPG reached a $\Phi_{p\text{-max}}$ of 900, and MDEA only produced a value of 600, all of them at around 38% conversion of vinyl groups. It is worth noting that Φ_p varies only slightly before the polymerization hits the gel effect (∼12.5 s and <4−5% conversion). These differences in Φ_p with amine should be associated with higher cross-linking densities due to higher initial concentration of primary radicals (with EDMAB), which leads to an enhanced effect of mobility in the termination constant (reaction-diffusion-controlled).[63,64,72]

While the reactivity trends of Φ_p and $\Phi_i/\Phi_{i\text{-ref}}$ were confirmed to be EDMAB > NPG > MDEA, we show that NPG > MDEA ≥ EDMAB in terms of initial Φ_{red} (Figure 4b). This difference could be attributed to alternate decomposition pathways, such as hydrogen abstraction from the alcohol or the carboxylic groups and N−H bonds in MDEA and NPG, respectively. These alternate hydrogen abstraction routes could lead to faster photoreduction rates, but the primary radicals produced therefrom can have a significantly lower efficiency in initiating polymerization than the α-aminoalkyl radicals that are typically produced. Alternatively, it is also likely that the concentration of primary radicals produced by the amine reductants is roughly equivalent, but that the α-aminoalkyl radicals from EDMAB are more reactive toward the vinyl groups than those from MDEA and NPG. Herein, we emphasize the potential of our UV−vis/FT−NIR technique for attaining more detailed analysis of these subtle differences in reactivity that can change as a function of reaction time and cannot be elucidated with other instruments.

3.3. Polymerization Kinetics Accounting for Difference in I_{abs}. Assuming that the pseudo-steady-state approximation is valid and that primary radical termination is negligible, a standard model for R_p has been well-established.[63,64,73,74] This model was utilized by Anseth et al. to determine the propagation (k_p) and termination (k_t) constants using a combination of steady-state and non-steady-state experiments with photo-DSC. These experiments were performed under the assumption that the rate of monomer initiation (R_i) remains constant. This assumption is most often only valid at the very early stages of the reaction, and thus could lead to inaccuracies at the later stages. Our UV−vis−FT−NIR device allows the same steady-state analysis $(k_p f^{1/2})/k_t^{1/2}$ without assuming constant R_i, thus permitting the estimation of k_p and k_t for a broader set of formulations and conditions (Figure 5c).

$$R_p = \left(\frac{k_p}{k_t^{1/2}}\right)[M]R_i^{1/2}$$

where

$$R_i = f\phi_{red}I_{abs}$$

$$\frac{R_p}{[M](I_{abs}\phi_{red})^{1/2}} = \left(\frac{k_p}{k_t^{1/2}}\right)f^{1/2}$$

where f is the fraction of primary radicals that lead to propagating monomer-based radicals and [M] is the concentration of vinyl groups. Here, R_p, I_{abs}, Φ_{red}, and [M] are time-dependent variables determined from the same experiment. Higher initial viscosity of the monomer(s) leads to higher R_p's due to diffusion-controlled and reaction-diffusion-controlled termination. Our results confirm that $(k_p f^{1/2})/k_t^{1/2}$ correlates linearly with ln(viscosity), where initial viscosities are 0.0175, 0.0356, and 0.7750 Pa·s for 0, 50, and 100 vol % EBADMA.[67,73] Non-steady-state kinetic experiments can also be accommodated in the UV−vis/FT−NIR apparatus but are beyond the scope of this introductory study.

3.4. Calculation of Photosensitivity and Residual Initiator. A photosensitivity (S) term is utilized as an efficiency parameter for light-activated polymerizations based on the amount of light energy absorbed during the time it takes to polymerize half of the functional groups ($t^{1/2}$) for coatings, stereolithography, imaging, and electronics applications.[75] However, S is a function of I_{abs}, which limits its validity to the early stages of the polymerization. With our coupled UV−

DOI: 10.1021/acs.macromol.5b01685
Macromolecules 2015, 48, 6781−6790

vis/FT−NIR tool the amount of moles of photons (einsteins) absorbed by the initiator can be now easily estimated at any reaction time (Figure 5d). Hence, S can be calculated without assuming a constant absorption rate (I_{abs}), where I_{abs} depends on initiator concentration, irradiation intensity, and emission spectrum (Figure 3a). Figure 5d shows that EDMAB reductant uses photons more efficiently toward the polymerization of TEGDMA than NPG and MDEA, which is in agreement with the results for $\Phi_i/\Phi_{i\text{-ref}}$ and Φ_p. Real-time determination of S accounting for changes in I_{abs} is important for many applications, where light-induced polymerizations are evaluated based solely on R_p without standardizing I_{abs} values.

Lastly, both the residual amount of polymerizable groups and initiator (or catalyst) can be simultaneously deduced (Figure 5d) from the UV−vis/FT−NIR data. This is important because there is increasing attention in the biomedical and dental materials fields on reducing the cytotoxicity of *in situ* or *in vivo* polymerized materials. For instance, residual CQ, MDEA, NPG, and EDMAB are known to be mutagenic leachable compounds that reduce the stability of dental restorative and adhesive materials.[55,76,77] Quantification of these residues is normally done postpolymerization and requires laborious extraction of the small molecules. Our technique permits direct deduction of residual vinyl groups and CQ concentrations for example, from the initiation and polymerization concentration data, thus potentially expediting formulation design and optimization. Residual amine reductant concentrations for these cases could then be inferred using mechanistic assumptions. While this technique does not directly measure residual free monomer content, this approach allows selection of irradiation conditions and initial concentrations that rationally minimize residual free monomer and initiator.

4. CONCLUSIONS

Rates of light absorption as well as initiator and monomer consumption were simultaneously tracked via coupled UV−vis/FT−NIR spectroscopy for the first time. To permit the kinetic analysis of multiple reaction steps in the polymerization process from a single set of experiments carried out in the polymerizing medium under the same conditions, we confirmed well-established trends and values for the effects of light intensity, initial concentrations, viscosity, and amine reductant chemistry. Then, we calculated key parameters that cannot be practically determined with other analytical tools: the conversion-dependent quantum yields of CQ photoreduction, initiation, and polymerization. We proved that the quantum yield of initiator consumption could be significantly affected by the mobility of the forming macromolecular architecture. This UV−vis/FT−NIR device can also extract the kinetic constants of propagation and termination without assuming a constant rate of initiation as well as the photosensitivity term used in many applications. Lastly, the residual initiator can be determined to evaluate the potential toxicity of a given formulation. While the relatively slow polymerizations discussed here do not showcase the millisecond time resolution of the UV−vis and FT−NIR detectors, there are a myriad of photopolymer formulations for which this capability can be invaluable. This opens interesting possibilities for accelerated elucidation of the mechanisms involved in a wide range of polymer syntheses including ATRP, RAFT, CuAAC, thiol−Michael, and thiol−ene, for which new and complex light-activated initiators and catalysts are currently being developed. This methodology can also provide detailed information to resolve the individual contributions of mixed photoinitiators operating at different wavelengths.

■ ASSOCIATED CONTENT

Supporting Information

The Supporting Information is available free of charge on the ACS Publications website at DOI: 10.1021/acs.macromol.5b01685.

Spectral processing of UV−vis data with MATLAB fitting and baseline shift due primarily to Rayleigh scattering, example of raw data with MATLAB fitting including differential equations for the kinetics of CQ and monomer consumption, change of optical properties of CQ chromophore as a function of solvent, comparison of UV−vis absorbance for equimolar solutions of CQ, NPG, and CQ/NPG in TEGDMA (PDF)

■ AUTHOR INFORMATION

Corresponding Author

*E-mail Jeffrey.Stansbury@ucdenver.edu (J.W.S.).

Funding

This work was supported by NIH/NIDCR R01DE014227, the NSF Industry/University Cooperative Research Center for Fundamentals and Applications of Photopolymerization, and CONACYT (Consejo Nacional de Ciencia y Tecnología) 308269.

Notes

The authors declare no competing financial interest.

■ REFERENCES

(1) Hawker, C. J.; Wooley, K. L. *Science* **2005**, *309*, 1200−1205.
(2) Wang, J.-S.; Matyjaszewski, K. *J. Am. Chem. Soc.* **1995**, *117*, 5614−5615.
(3) Barner-Kowollik, C.; Lutz, J. F.; Perrier, S. *Polym. Chem.* **2012**, *3*, 1677−1679.
(4) Gong, T.; Adzima, B. J.; Bowman, C. N. *Chem. Commun.* **2013**, *49*, 7950−7952.
(5) Hoyle, C. E.; Bowman, C. N. *Angew. Chem., Int. Ed.* **2010**, *49*, 1540−1573.
(6) Patterson, G. D. *Annu. Rev. Mater. Sci.* **1983**, *13*, 219−245.
(7) Boiko, Y. B.; Granchak, V. M.; Dilung, I. I.; Tikhonov, E. A. *J. Appl. Spectrosc.* **1990**, *52*, 149−153.
(8) Drenski, M. F.; Mignard, E.; Alb, A. M.; Reed, W. F. *J. Comb. Chem.* **2004**, *6*, 710−716.
(9) Désilles, N.; Gautrelet, C.; Lecamp, L.; Lebaudy, P.; Bunel, C. *Eur. Polym. J.* **2005**, *41*, 1296−1303.
(10) Mignard, E.; Lutz, J.-F.; Leblanc, T.; Matyjaszewski, K.; Guerret, O.; Reed, W. F. *Macromolecules* **2005**, *38*, 9556−9563.
(11) Chang, S. Y.; Chang, S. Y.; Wang, N. S.; Wang, N. S. *Monitoring Polymerization Reactions by Near-IR Spectroscopy*; ACS Symposium Series; American Chemical Society: Washington, DC, 1995.
(12) Florenzano, F. H.; Strelitzki, R.; Reed, W. F. *Macromolecules* **1998**, *31*, 7226−7238.
(13) Reed, W. F. *Macromolecules* **2000**, *33*, 7165−7172.
(14) Alb, A. M.; Mignard, E.; Drenski, M. F.; Reed, W. F. *Macromolecules* **2004**, *37*, 2578−2587.
(15) Alb, A. M.; Serelis, A. K.; Reed, W. F. *Macromolecules* **2008**, *41*, 332−338.
(16) Decker, C.; Moussa, K. *Makromol. Chem.* **1988**, *189*, 2381−2394.
(17) Esen, D. S.; Karasu, F.; Arsu, N. *Prog. Org. Coat.* **2011**, *70*, 102−107.
(18) Cherdoud-Chihani, A.; Mouzali, M.; Abadie, M. *Eur. Polym. J.* **1997**, *33*, 969−975.

DOI: 10.1021/acs.macromol.5b01685
Macromolecules 2015, 48, 6781−6790

(19) Allonas, X.; Lalevée, J.; Fouassier, J. P. *Photoinitiated Polymerization*; ACS Symposium Series; American Chemical Society: Washington, DC, 2009; Vol. *847*, pp 140−151.
(20) Roper, T. M.; Guymon, C. A.; Hoyle, C. E. *Rev. Sci. Instrum.* **2005**, *76*, 054102.
(21) Crivello, J. V. *J. Polym. Sci., Part A: Polym. Chem.* **2009**, *47*, 866−875.
(22) Fonseca, G. E.; Dubé, M. A.; Penlidis, A. *Macromol. React. Eng.* **2009**, *3*, 327−373.
(23) Stansbury, J. W.; Dickens, S. H. *Dent. Mater.* **2001**, *17*, 71−79.
(24) Decker, C.; Moussa, K. *Macromolecules* **1989**, *22*, 4455−4462.
(25) Darcos, V.; Monge, S.; Haddleton, D. M. *J. Polym. Sci., Part A: Polym. Chem.* **2004**, *42*, 4933−4940.
(26) Decker, C.; Moussa, K. *Makromol. Chem., Rapid Commun.* **1990**, *11*, 159−167.
(27) Decker, C. *UV-Curing Chemistry: Past, Present, and Future*; JCT: 1987; Vol. *59*, pp 97−106.
(28) Moussa, K.; Decker, C. *J. Polym. Sci., Part A: Polym. Chem.* **1993**, *31*, 2197−2203.
(29) Decker, C. *Prog. Polym. Sci.* **1996**, *21*, 593−650.
(30) Mark, H.; Campbell, B. *An Introduction to near Infrared Spectroscopy and Associated Chemometrics*; The Near Infrared Research Corporation: 2008.
(31) Asmusen, S.; Arenas, G.; Cook, W. D.; Vallo, C. *Dent. Mater.* **2009**, *25*, 1603−1611.
(32) Asmussen, S.; Arenas, G.; Cook, W. D.; Vallo, C. *Eur. Polym. J.* **2009**, *45*, 515−522.
(33) Fouassier, J.-P.; Morlet-Savary, F.; Lalevée, J.; Allonas, X.; Ley, C. *Materials* **2010**, *3*, 5130−5142.
(34) Lalevée, J.; Blanchard, N.; Tehfe, M.-A.; Peter, M.; Morlet-Savary, F.; Fouassier, J. P. *Macromol. Rapid Commun.* **2011**, *32*, 917−920.
(35) Timpe, H.-J.; Kronfeld, K.-P.; Lammel, U.; Fouassier, J. P.; Lougnot, D.-J. *J. Photochem. Photobiol., A* **1990**, *52*, 111−122.
(36) Allonas, X.; Lalevée, J.; Fouassier, J. P. *Chem. Phys.* **2003**, *290*, 257−266.
(37) Tehfe, M.-A.; Lalevée, J.; Telitel, S.; Sun, J.; Zhao, J.; Graff, B.; Morlet-Savary, F.; Fouassier, J. P. *Polymer* **2012**, *53*, 2803−2808.
(38) Lalevée, J.; Blanchard, N.; El-Roz, M.; Graff, B.; Allonas, X.; Fouassier, J. P. *Macromolecules* **2008**, *41*, 4180−4186.
(39) Allonas, X.; Lalevée, J.; Fouassier, J. P. *J. Photochem. Photobiol., A* **2003**, *159*, 127−133.
(40) Treat, N. J.; Sprafke, H.; Kramer, J. W.; Clark, P. G.; Barton, B. E.; Read de Alaniz, J.; Fors, B. P.; Hawker, C. J. *J. Am. Chem. Soc.* **2014**, *136*, 16096−16101.
(41) Tehfe, M.-A.; Lalevée, J.; Morlet-Savary, F.; Graff, B.; Blanchard, N.; Fouassier, J. P. *ACS Macro Lett.* **2012**, *1*, 198−203.
(42) Worrell, B. T.; Malik, J. A.; Fokin, V. V. *Science* **2013**, *340*, 457−460.
(43) Aguirre-Soto, A.; Lim, C.-H.; Hwang, A. T.; Musgrave, C. B.; Stansbury, J. W. *J. Am. Chem. Soc.* **2014**, *136*, 7418−7427.
(44) Long, M.; Rogers, S. H.; Thornthwaite, D. W.; Livens, F. R.; Rannard, S. P. *Polym. Chem.* **2011**, *2*, 581−589.
(45) Chen, Y.-C.; Ferracane, J. L.; Prahl, S. A. *Dent. Mater.* **2007**, *23*, 655−664.
(46) Schmitt, M. *Macromol. Chem. Phys.* **2011**, *212*, 1276−1283.
(47) Alakhras, F.; Holze, R. *Synth. Met.* **2007**, *157*, 109−119.
(48) Lamps, J. P.; Catala, J. M. *Macromolecules* **2011**, *44*, 7962−7968.
(49) Meinwald, J.; Klingele, H. O. *J. Am. Chem. Soc.* **1966**, *88*, 2071−2073.
(50) Monroe, B. M.; Weiner, S. A. *J. Am. Chem. Soc.* **1969**, *91*, 450−456.
(51) Monroe, B. M.; Weiner, S. A. *J. Am. Chem. Soc.* **1968**, *90*, 1913−1914.
(52) Neumann, M. G.; Miranda, W. G., Jr.; Schmitt, C. C.; Rueggeberg, F. A.; Correa, I. C. *J. Dent.* **2005**, *33*, 525−532.
(53) Decker, C. *J. Polym. Sci., Part A: Polym. Chem.* **1992**, *30*, 913−928.
(54) Pączkowski, J.; Neckers, D. C. *Macromolecules* **1992**, *25*, 548−553.
(55) Ilie, N.; Hickel, R. *Dent. Mater. J.* **2008**, *27*, 221−228.
(56) Stansbury, J. W. *J. Esthet Dent* **2000**, *12*, 300−308.
(57) Cook, W. D.; Chen, F. *J. Polym. Sci., Part A: Polym. Chem.* **2011**, *49*, 5030−5041.
(58) Cook, W. D. *Polymer* **1992**, *33*, 600−609.
(59) Jakubiak, J.; Allonas, X.; Fouassier, J. P.; Sionkowska, A. *Polymer* **2003**, *44*, 5219−5226.
(60) Ikemura, K. K.; Ichizawa, K. K.; Yoshida, M. M.; Ito, S. S.; Endo, T. T. *Dent. Mater. J.* **2008**, *27*, 765−774.
(61) Pyszka, I.; Kucybala, Z. A.; Paczkowski, J. *Macromol. Chem. Phys.* **2004**, *205*, 2371−2375.
(62) Xi, W.; Peng, H.; Aguirre-Soto, A.; Kloxin, C. J.; Stansbury, J. W.; Bowman, C. N. *Macromolecules* **2014**, *47*, 6159−6165.
(63) Anseth, K. S.; Wang, C. M.; Bowman, C. N. *Polymer* **1994**, *35*, 3243−3250.
(64) Anseth, K. S.; Kline, L. M.; Walker, T. A.; Anderson, K. J.; Bowman, C. N. *Macromolecules* **1995**, *28*, 2491−2499.
(65) Davidenko, N.; García, O.; Sastre, R. *J. Appl. Polym. Sci.* **2005**, *97*, 1016−1023.
(66) Abu-elenain, D. A.; Lewis, S. H.; Stansbury, J. W. *Dent. Mater.* **2013**, *29*, 1173−1181.
(67) Dickens, S. H.; Stansbury, J. W.; Choi, K. M.; Floyd, C. J. E. *Macromolecules* **2003**, *36*, 6043−6053.
(68) García, N.; Tiemblo, P.; Guzmán, J. *Macromolecules* **2007**, *40*, 4802−4808.
(69) García, N.; Tiemblo, P.; Hermosilla, L.; Calle, P.; Sieiro, C.; Guzmán, J. *Macromolecules* **2007**, *40*, 8168−8177.
(70) Olaj, O. F.; Vana, P. *J. Polym. Sci., Part A: Polym. Chem.* **2000**, *38*, 697−705.
(71) Fouassier, J. P.; Lalevée, J. *Photoinitiators for Polymer Synthesis: Scope, Reactivity, and Efficiency*, 1st ed.; Wiley-VCH: Weinheim, 2012.
(72) Anseth, K. S.; Rothenberg, M. D.; Bowman, C. N. *Macromolecules* **1994**, *27*, 2890−2892.
(73) Lovell, L. G.; Stansbury, J. W.; Syrpes, D. C.; Bowman, C. N. *Macromolecules* **1999**, *32*, 3913−3921.
(74) Anseth, K. S.; Wang, C. M.; Bowman, C. N. *Macromolecules* **1994**, *27*, 650−655.
(75) Sugawara, S. S.; Murase, K. K.; Kitayama, T. T. *Appl. Opt.* **1975**, *14*, 378−382.
(76) Atsumi, T.; Iwakura, I.; Fujisawa, S.; Ueha, T. *Arch. Oral Biol.* **2001**, *46*, 391−401.
(77) Tseng, W.-Y.; Huang, C.-H.; Chen, R.-S.; Lee, M.-S.; Chen, Y.-J.; Rueggeberg, F. A.; Chen, M.-H. *J. Biomed. Mater. Res., Part B* **2007**, *83*, 85−90.

DOI: 10.1021/acs.macromol.5b01685
Macromolecules 2015, 48, 6781−6790